ARMY RESEARCH LABORATORY

Investigation of Small-Caliber Primer Function Using a Multiphase Computational Model

by John R. Schmidt and Michael J. Nusca

ARL-TR-4514   **July 2008**

NOTICES

Disclaimers

The findings in this report are not to be construed as an official Department of the Army position unless so designated by other authorized documents.

Citation of manufacturer's or trade names does not constitute an official endorsement or approval of the use thereof.

Destroy this report when it is no longer needed. Do not return it to the originator.

Army Research Laboratory

Aberdeen Proving Ground, MD 21005-5066

ARL-TR-4514 **July 2008**

Investigation of Small-Caliber Primer Function Using a Multiphase Computational Model

John R. Schmidt and Michael J. Nusca
Weapons and Materials Research Directorate, ARL

REPORT DOCUMENTATION PAGE

Form Approved
OMB No. 0704-0188

1. REPORT DATE *(DD-MM-YYYY)*	2. REPORT TYPE	3. DATES COVERED *(From - To)*
July 2008	Final	

4. TITLE AND SUBTITLE	5a. CONTRACT NUMBER
Investigation of Small-Caliber Primer Function Using a Multiphase Computational Model	
	5b. GRANT NUMBER
	5c. PROGRAM ELEMENT NUMBER
6. AUTHOR(S)	5d. PROJECT NUMBER
John R. Schmidt and Michael J. Nusca	
	5e. TASK NUMBER
	5f. WORK UNIT NUMBER

7. PERFORMING ORGANIZATION NAME(S) AND ADDRESS(ES)	8. PERFORMING ORGANIZATION REPORT NUMBER
U.S. Army Research Laboratory Weapons and Materials Research Directorate ATTN: AMSRD ARL WM BD Aberdeen Proving Ground, MD 21005-5066	ARL-TR-4514

9. SPONSORING/MONITORING AGENCY NAME(S) AND ADDRESS(ES)	10. SPONSOR/MONITOR'S ACRONYM(S)
	11. SPONSOR/MONITOR'S REPORT NUMBER(S)

12. DISTRIBUTION/AVAILABILITY STATEMENT

Approved for public release; distribution is unlimited.

13. SUPPLEMENTARY NOTES

14. ABSTRACT

This report describes further development in the formulation of a primer model that is compatible with the ARL-NGEN3 code and small-caliber weapons that takes in account multidimensional, multiphase interior ballistics codes, which employ coupled Eulerian-Lagrangian schemes to explicitly treat both the gas and solid phase. The model is based on the One Dimensional Turbulence modeling approach that has recently emerged as a powerful tool in multiphase simulations. Initial results are shown for the model run as a stand-alone code and are compared to recent experiments with small-caliber primers. Integration of the primer model with the Army's ARL-NSRG computational fluid dynamics code is presented and the results are compared to experiments with small-caliber primers fired into empty test chambers. It is proposed that this further progress sets the stage for coupling the primer model to the ARL-NGEN3 code.

15. SUBJECT TERMS

Interior ballistics, Turbulence, Primer, CFD, two-phase flow

16. SECURITY CLASSIFICATION OF:			17. LIMITATION OF ABSTRACT	18. NUMBER OF PAGES	19a. NAME OF RESPONSIBLE PERSON
a. REPORT	**b. ABSTRACT**	**c. THIS PAGE**	UU	36	John R. Schmidt
U	U	U			19b. TELEPHONE NUMBER *(Include area code)* (410) 278-5510

Contents

List of Figures

Acknowledgments

INTENTIONALLY LEFT BLANK.

1. Introduction

Numerical simulation of the interior ballistics (IB) of large-caliber guns has steadily progressed over the last few decades. As a testament to this progress, the U.S. Army Research Laboratory (ARL) (known prior to 1992 as the Ballistics Research Laboratory (BRL)) has played a major role in the development and popularization of a number of IB codes, such as IBHVG2 (*1*), NOVA (also known as XKTC) (*2*, *3*), and NGEN (*4–6*), with progress in both model complexity and dimensionality (i.e., 0-dimensional (D), 1-D, and 2-D/3-D, respectively). A good review of the utility of this suite of IB codes is given by Horst and Nusca (*7*). Through this ambitious and successful progression of IB code development, one area of research has been given less attention: the fidelity with which the ignition system (i.e., the primer in small-caliber guns, the primer and flashtube in medium-caliber guns, and the primer and igniter-tube in large-caliber guns) is represented. One notable exception is an igniter sub-model implemented in the NOVA code for a 105 mm tank gun charge of low vulnerability gun propellant (*8*, *9*). In this model the primer efflux was treated as gaseous with an added condensing phase, which increases the heat transfer coefficient to the propellant.

There is significant evidence that burning particles of various chemical compositions and sizes are ejected from gun primers (*10–12*) and interact with the propellant grains during charge ignition. It is perhaps due to this phenomenon that upgrades to IB codes in this regard have had to wait until IB codes were made to utilize an explicit, particle-based treatment of the propellant. It follows that such an IB code could be made to model the interaction of the discrete primer particles and the discrete propellant particles. With the advent of the ARL-NGEN3 IB code, which employs a coupled Eulerian-Lagrangian scheme to explicitly treat both the continuous (gases) and discrete (solid) phases, the time is ripe for a primer model that is commensurate with the availability of such an IB model.

Such a primer model has been developed, has been described previously (*13*, *14*), and will be summarized herein. As a first stage of testing, calibrating, and ultimately validating this primer model, this report describes an effort to couple this model to a general purpose computational fluid dynamics (CFD) code called ARL-Navier-Stokes Real Gas (NSRG), and then shows how this combined model is used to simulate data gathered in a carefully designed ballistic simulator for the small-caliber ammunition. The lessons learned will assist in guiding the ultimate goal of coupling the primer model to the ARL-NGEN interior ballistics code for the purpose of a complete simulation of small-caliber ammunition (figure 1).

Figure 1. Cut away of a 5.56-mm small-caliber round.

2. Previous Work

Previous reports (*13*, *14*) detailed the initial work toward the development of a small-caliber primer model. Provided herein is a summary of that work.

A literature search was performed to understand the function of the percussion primer and glean the importance and purpose of each of the ingredients in the No. 41 primer. Overall chemical reactions for the species were derived. National Aeronautics and Space Administration (NASA)-Glenn thermodynamic calculations were performed as a check of all the major species formed at one atmosphere pressure. Cheetah thermodynamics calculations were preformed under gun conditions to determine the ideal combustion state for the exploded primer. These conditions are needed for IB calculations. This state was used to estimate physical constants of the gas phase, which were used for the particle-laden One Dimensional Turbulence (ODT) simulations. It was proposed that the primer could be satisfactorily modeled as a highly turbulent statistically steady-state constant density particle-laden channel flow using one-way coupling. The material coming out of the primer tube, before the propellant is ignited, was determined to be (1) the gas phase, consisting of the combustion products of lead styphnate, Tetracene, pentaerythritoltetranitrate (PETN), and aluminum; (2) the solid phase, determined to be the uncombusted barium nitrate and antimony sulfide; and (3) a condensed phase, indicated by a thermochemical calculation.

It was determined that only the drag terms of the particle equation of motion were significant and particles hitting the wall would stick to the wall rather than bounce off the wall. A channel flow with a bulk Reynolds number (Re) of approximately 12,000 was chosen to simulate the flow. A brief overview of vector ODT with two-phase flow as it pertains to this application was given. The deposition velocity V_d^+ was calculated for small particle size and compared to literature values for V_d^+. Excellent agreement was achieved for the small radii simulations, but a new diameter dependence of V_d^+ was noted. Mean particle velocity profiles across the ODT channel yielded close agreement with measured particle velocities.

3.   Small-Caliber Ammunition Chamber Simulator

The modeling phase of this project was done in close coordination with the experimentation of Williams et al. (*15*, *16*). Their work consisted of the following:

1. They performed open air primer firing events with high-speed digital photography (figure 2). From this, they were able to measure particle exit velocities. Analysis of the photograph revealed a spreading angle of ~70°. Two yellow lines were placed in the photograph to show the 70° spreading angle.
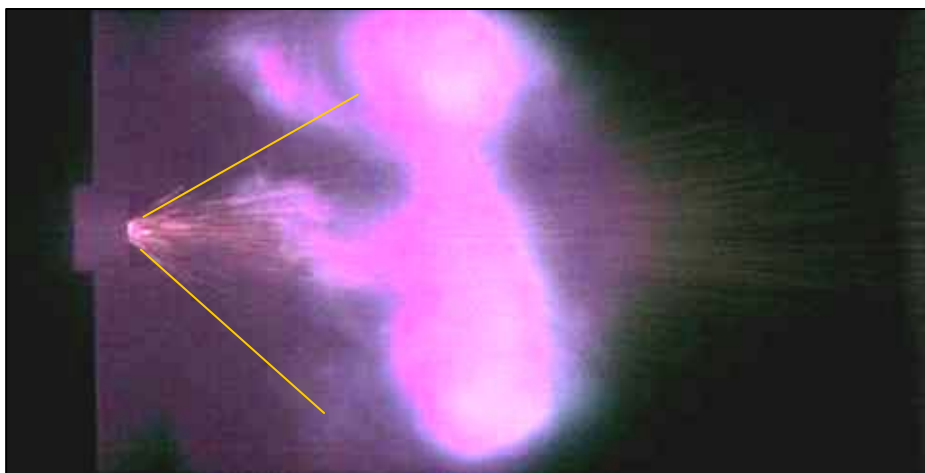
Figure 2. Primer No. 41 open air firing.

Note: Taken from Williams et al. (*16*) with permission.

2. They collected particles from the open air primer firings. Samples were collected on carbon tape and analyzed using Scanning Electron Microscopy/Energy-Dispersive X-ray spectroscopy (SEM/EDAX) Fourier Transform Infrared (FTIR) spectroscopy. The impetus behind these experiments was to try and find out what was coming out of the primer spit hole at the very beginning of the ballistic cycle. During the ballistic event, the primer efflux ignites the propellant, which increases the pressure and temperature inside the gun case. Firing primers into open air is, in effect, quenching the reaction just after the initiation, because the products are spit out of the primer tube into room temperature and pressure. Their conclusions were that the solids coming out of the primer tube were particles of barium nitrate and antimony sulfide with evidence of some melting and perhaps a small level of combustion. Traces of mostly sub-micron aluminum/aluminum oxide were noted, the authors of this report attribute this to the aerosol generation from the gaseous state due to the quenching of the hot gases as they were shot into the open air (which was at room temperature and pressure).

3. They developed a closed ballistic simulator made of clear acrylic, which was used to test the firing of the No. 41 primer into an empty chamber. Time dependent pressure measurements of the projectile end of the simulator were taken in conjunction with high speed photography of the firing event as could be seen through the acrylic sidewalls. A high frequency pressure wave was noted due to the complex interactions between multiple wave fronts reflecting between the two chamber ends. The signal was filtered. The chamber pressure reached a maximum value of about 3 MPa in a time of between 25 and 35 microseconds. A schematic diagram of the primer and empty chamber is shown in figure 3. A pressure time curve is shown in figure 4.
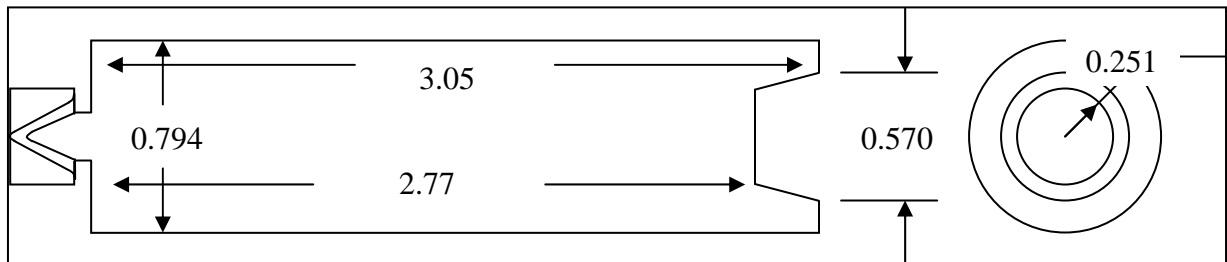
Figure 3. The 5.56 ballistic simulator, where the channel between the primer (on the left) and the simulator is .203 cm in diameter and .165 cm deep, respectively, and the simulator volume is 1.45 cc.

Note: All measurements in units of cm.
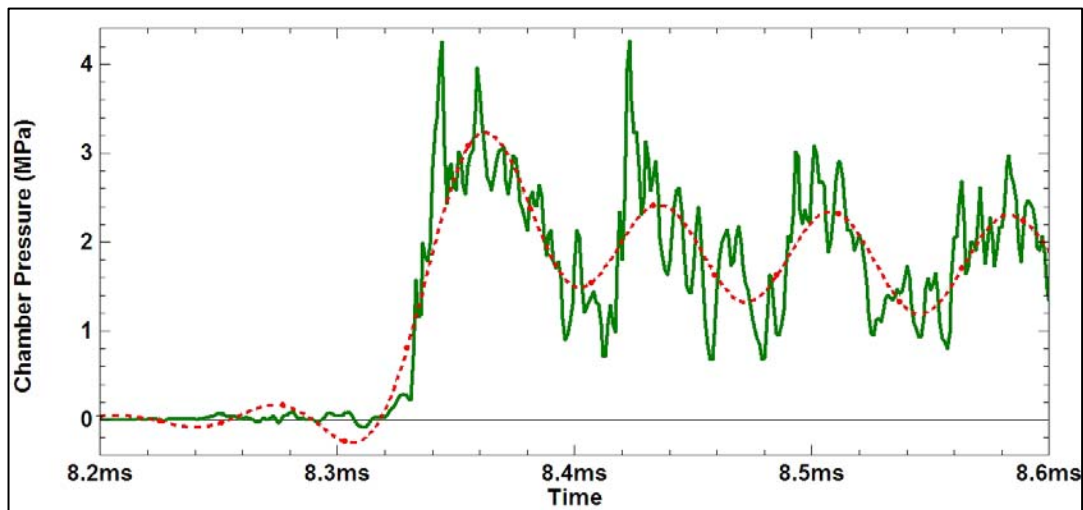
Figure 4. A measured pressure time curve of the empty ballistic simulator chamber (with and without a 15-kHz low-pass filter).

Note: The dashed line shows the filtered curve. Taken from Williams et al. (*16*) with permission.

4. They utilized the closed ballistic simulator for experiments with both inert propellant and live propellant. Time dependent pressure measurements and high speed photography were performed. Analysis done postmortem on the inert propellant balls supported the supposition that the open air firing quenched the reaction soon after the primer firing.

Comparison of the analytical results of the open air firings and the closed chamber firings showed that there was further reaction in the closed chamber, which had a peak pressure of 18.3 MPa as compared to the open air firings where the pressure was atmospheric (~0.1 MPa). This is consistent with the use of barium nitrate and antimony sulfide in primer to extend the life of the primer. That is, they continue to burn after the firing event to provide extra heat to ignite the propellant. The live propellant simulations will be used in future work to help verify the ARL-NGEN code extension to small-caliber IB.

4. Multi-Species, Multi=Phase Flow CFD Code

The ARL-NSRG CFD code is a time-accurate, multi-dimensional CFD code that has been under development and validation at ARL for over 10 years (*17*). This code has been successfully used for the simulation of unsteady, multi-component, turbulent, chemically reacting (nonequilibrium) flows (*18–23*). The code solves the unsteady Navier-Stokes equations, including multicomponent species diffusion, thermal conduction, viscosity (laminar and turbulent), and user-defined nonequilibrium chemical kinetics. The conservation-law form of the Navier-Stokes equations is used and a finite-volume discretization methodology is employed. The convective and transport fluxes are resolved using upwind and central-differencing along with flux-limiting methods. The chemical reactions are fully coupled to the gas dynamics and the numerical stiffness due to chemical source terms is mitigated by pre-conditioning techniques, thus permitting explicit time integration (i.e., a technique that accurately represents wave dynamics). Several kinetics mechanisms have been installed in the code using an Arrhenius formulation (the code admits other methods for computing the chemical source terms including pressure-dependent and "falloff" reaction rates). Real-gas equations of state (e.g., Noble-Abel, Jones-Wilkins-Lee (JWL), and Peng-Robinson) are also available in the code. Although originally formulated for gas-phase modeling, the ARL-NSRG code has been recently upgraded to include a discrete phase, which can be either liquid or solid. This version of the code has been successfully used for the modeling of liquid rocket engines (*22*, *23*). The multiphase version of the code includes governing equations to simulate particle dynamics (including interphase drag and heat conduction), particle heating and vaporization, as well as the participation of these particles in chemical reactions if so desired.

Particularly germane to the current application of the code is a similar application in which the ARL-NSRG CFD code was coupled to a model that predicted the efflux from the orifice of a capillary containing a solid material (polyethylene) that was vaporized when high-voltage current was applied to the leads of an included copper wire. The resulting efflux was a high velocity, high density, chemical mixture primarily composed of electrons, C, C+, H, H+, and other species. This efflux, in the form of a highly underexpanded jet, was exhausted into a chamber containing air and a solid propellant sample. The ARL-NSRG CFD code was used to

5

resolve this jet. Output of the capillary model was used as a boundary condition for the ARL-NSRG, which produced resultant shock waves at the orifice (the classical barrel shocks, normal shock, and reflected shocks) and the subsequent series of shock wave reflections within the test chamber. Measured and computed pressure/time histories were compared. In this case, the code included a nonequilibrium chemical kinetics mechanism (air-plasma-JA2 propellant) and certain real fluid effects (Coulomb interactions) that are present for ionized gases. For further details on the model and results, refer to the work of Nusca, McQuaid, and Anderson (*19–21*). The overall plasma-propellant interaction research program is described by Shaw et al. (*24*). Clearly, the current application of the ARL-NSRG CFD code is quite similar to this previous case since a primer model will be used to supply the CFD code with the flow properties and conditions at the primer orifice that is issuing into a closed chamber as a boundary condition.

5. Primer Model and Interface to CFD Code

There exist a number of challenges in order to couple the ODT two-phase flow model with the ARL-NGEN code. An important first step is the merging of the ODT with the ARL-NSRG code. Analysis of the Military (Mil) specifications (Mil-A-159, Class 1, 2, and 3) for the antimony sulfide and (Mil-B-162, Class 1 granulation A) for barium nitrate were performed. A log averaged mean diameter of 95 microns was found suitable for both antimony sulfide (Stokes number $\tau p+ = 28{,}000$) and barium nitrate ($\tau p+ = 19{,}600$). Assuming a 95 micron diameter particle, the total number of barium nitrate particles in an average No. 41 primer is calculated to be 5,493; for stibnite, the calculation yields 1,800 particles.

Grid convergence studies were performed at 1,292 and 2,584 grid points. The statistical steady-state deposition velocity V_d+ was calculated and it was confirmed that 1,292 grid points were of sufficient resolution.

An example of a Re = 356 steady-state fluid velocity profile across the channel is shown in figure 5, where the wall-normal direction is denoted y. Mean V and W fluid velocity profiles are zero. Also shown is a transient fluid U velocity profile for comparison. The channel half height h is equal to 0.1016 cm. The friction velocity $U\tau$ is 2.81 m/s. The velocity at the centerline (y/h = 1) is equal to 55.7 m/s.
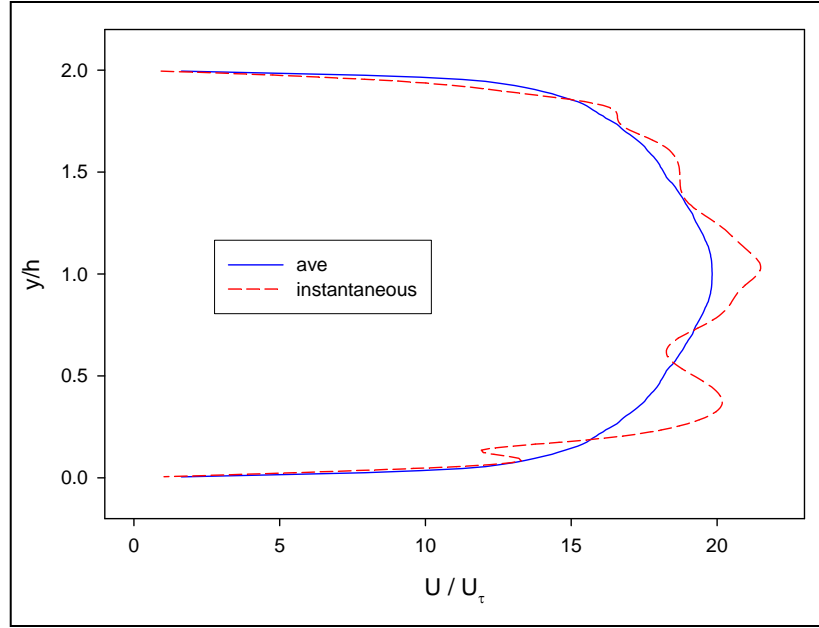
Figure 5.   Average and instantaneous ODT velocity profiles for Re_τ = 356;
the instantaneous profile was randomly chosen to demonstrate the
difference between mean velocity, computed for an ensemble and
arbitrary instantaneous velocity profile.

Note: The mean profile is the smooth one.

The Stokes number τp+ is the ratio of the aerodynamic time constant of the particle to the time constant (based on wall units) of the fluid. The closer the Stokes number is to 1, the more likely a particle is to follow the fluid. As the Stokes number becomes larger, the particle is less and less sensitive to its position across the channel, the wall-normal direction, here measured in wall units Y+ (*24*). Figure 6 shows the steady-state wall-normal profiles of particles with varying Stokes numbers: Lycopodium spores with τp+ = 10, glass beads with τp+ = 120, and copper shot with τp+ = 790. As can be seen in figure 5, the fluid velocity drops drastically near the wall. The Lycopodium spores with a Stokes number of 10 follow this trend quite readily. As the Stokes number goes up a factor of 10 (for glass), the slowing down of the particle's U velocity as it approaches the wall is attenuated. For the copper shot, which has a Stokes number two orders of magnitude higher, the wall effects are much less evident. Therefore one would expect minimal wall effect in U velocities for the particles of interest in this study, barium nitrate and antimony sulfide, which have Stokes numbers three orders of magnitude higher than Lycopodium spores.
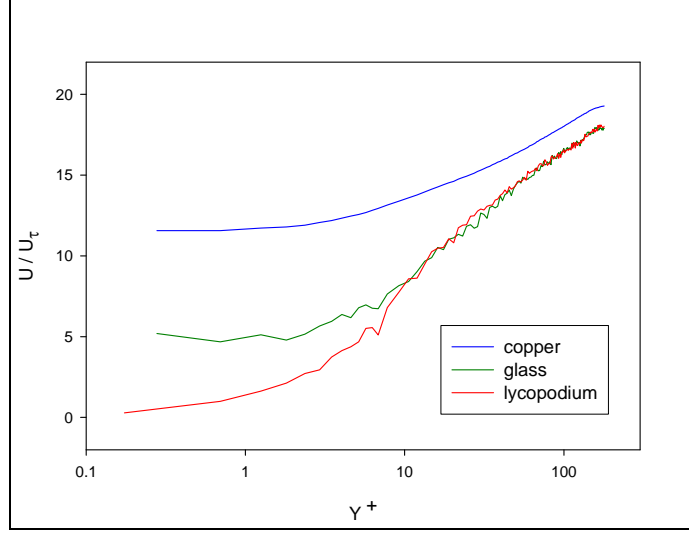
Figure 6.   ODT wall-normal profiles of wall-normalized stream-wise
             velocity U for copper shot (τp = 790), glass beads (τp = 120),
             and lycopodium spores (τp = 10) for Re_τ = 180.

Note: Taken from Schmidt (*25*) with permission.

Figure 7 shows the steady-state U velocity profile for barium nitrate as a function of the wall-normal direction. As expected, the slowing down of the particle as it approaches the wall is minimal. The mean particle velocity profiles in the Y and Z directions, V and W, respectively, are zero if the particles are allowed to bounce spectrally on the walls. If the particles are absorbed on the wall, then the mean V velocity profile shows a slight velocity toward the wall in the near wall region. This is due to fact that if they bounced off the wall they would contribute a velocity component away from the wall, but since they are absorbed on the wall there is a V velocity toward the wall. The antimony sulfide particle behavior is similar in every way to the barium nitrate particle. Only the antimony sulfide particles have a larger Stokes number, which means that it is even less sensitive to slowing in the near wall region.
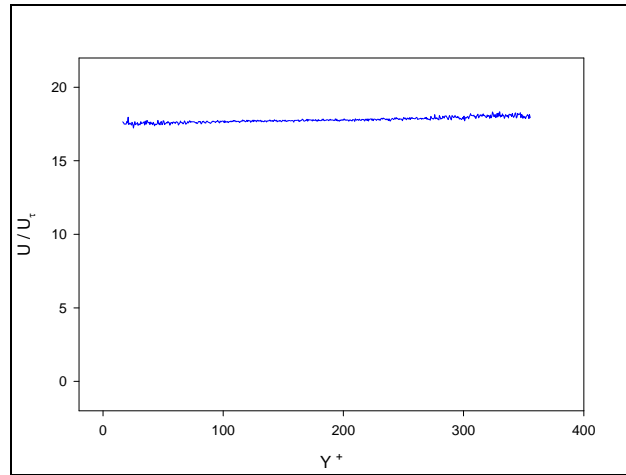

Figure 7. ODT wall-normal profiles of wall-normalized stream-wise
            velocity for barium nitrate (τ_p = 19,600) for Re$_\tau$ = 356.

8

To model the flow out of the primer tube into the ballistic simulator, the mean velocity profile for half the channel width (h) was fed into the ARL-NSRG simulation. The mean velocity profile is symmetric around the channel center. The vector ODT model provides instantaneous velocity profiles in the X, Y, and Z directions. The ARL-NSRG program uses the axis symmetric coordinate system R, θ, Z. The Z coordinate in ARL-NSRG corresponds to the X coordinate in the ODT code. Hence the stream-wise (U) velocity from ODT is the Z velocity for ARL-NSRG. Since ARL-NSRG assumes an axis-symmetric velocity profile, the θ velocity component is assumed to be zero. The ODT program models a 1-D line of sight on which the turbulent velocity profile is kept track of in all three dimensions. The θ component in ARL-NSRG corresponds in this case to the Z component in ODT. The R component in ARL-NSRG corresponds to the Y component in ODT. The V velocity profile corresponds to the R velocity.

Particles in ODT are allowed to migrate in their own individual space time line, so they have their own X, Y, Z, t position; however, all particles are constrained to stay on the ODT 1-D domain. Since the particles have their own Y, Z positions, an attempt was made to map the particle position and velocity into the R, θ coordinates. A total of 1,260 particles were released and allowed to reach pseudo-steady-state. The particles were binned into 10 equal time increments and converted into R, θ coordinates.

Particles in ARL-NSRG must be at least one diameter apart and cannot get within one radius of the walls. The ODT particles in each time bin were sorted in the R coordinate so that they were at least one radius apart. These efforts will hopefully bare fruit in future ARL-NSRG simulations.

6.   Results and Discussion

The computational domain chosen to simulate the ARL small-caliber ammunition experiment (as shown in figure 3) is shown in figure 8. The computational domain extends from the exit plane of the primer orifice (i.e., entrance to the simulator chamber) on the left, to the afterbody of the 5.56 ammunition mounted on the chamber sealing wall on the right (3.05 cm) and within the cylindrical wall of the chamber (which were made from a semi-transparent Lexan)—a diameter of 0.794 cm. This region was discretized using 304 axial grid cells and 40 radial grid cells (79 across the diameter), distributed with essentially even spacing throughout, as shown in figure 8 (partial grid deployed for clarity). Some degree of radial grid clustering was used among the chamber walls in order to more accurately resolve viscous effects. The boundary conditions for the region are non-slip/no-penetration on all solid walls along with specified inflow at the primer orifice (0.102 cm < Y < 0.102 cm at X = 0). Initially, the entire flowfield is filled with air (0.8 mole fraction of N2 and 0.2 mole fraction of O2) at standard pressure and temperature. During the simulation, a two-phase flow was fed into the chamber using the parameters described in section 5.
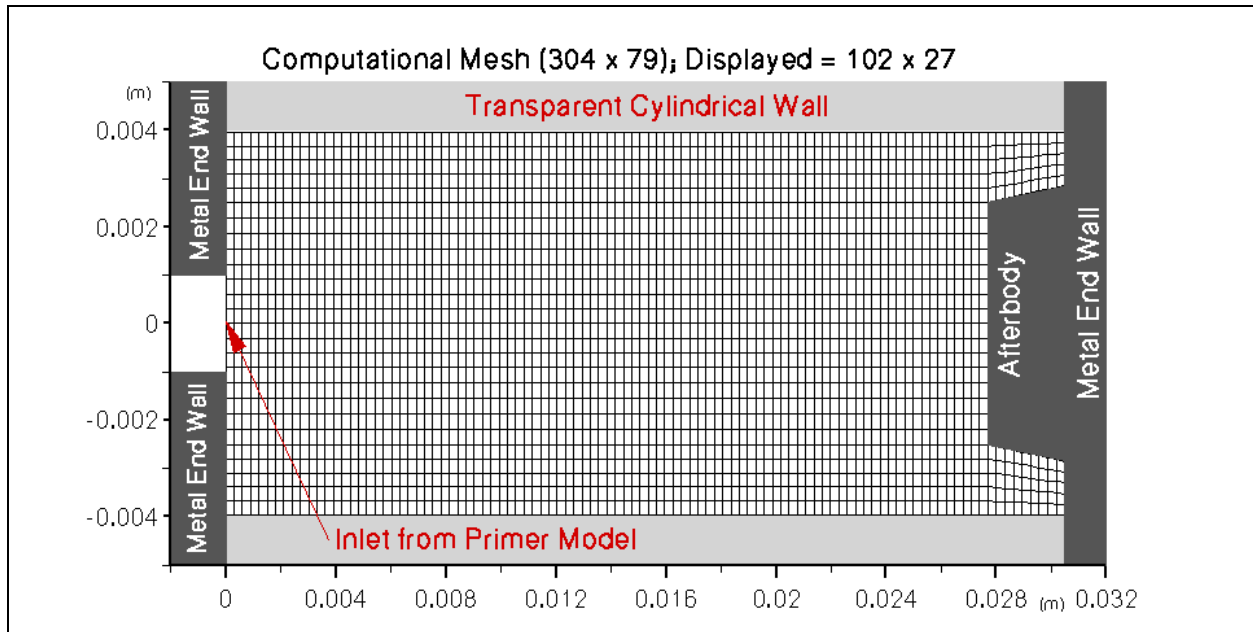
Figure 8. Computational mesh used for the simulation of the small-caliber ammunition simulator, as shown in figure 3; partial grid shown for clarity. Note the stretching (~1.5×) of the figure in the transverse.

The efflux from the 5.56 caliber ammunition primer into an empty chamber is postulated to resemble that of a high-speed, high-pressure jet that is said to be highly "underexpanded." To aid in the interpretation of computational results for the primer jet, figure 9 shows a schematic of the gas dynamic features expected in highly underexpanded supersonic jets (*21*). The efflux of primer from the inlet generates a weak precursor shock (A) that expands spherically. Behind this shock is air; the primer gases are entirely contained by this shock and are separated from the air by an irregularly shaped contact surface (B) across which pressure and velocity are preserved but entropy changes discontinuously. Expansion waves (Mach cone), generated at the inlet (C), travel to the precursor shock (A), are reflected as weak compression waves, and coalesce into a strong oblique shock, or barrel shock (D), within the primer jet. This barrel shock (D) terminates in an irregular reflection that forms a triple-point (E) joining the barrel shock (D) its reflection (F), and a normal shock (G) or Mach disk. Whereas the precursor shock (A) is relatively weak and diffuse, producing a mildly supersonic flow, the barrel shock (D) and Mach disk (G) are strong shocks that enclose a fully supersonic flow region.

10
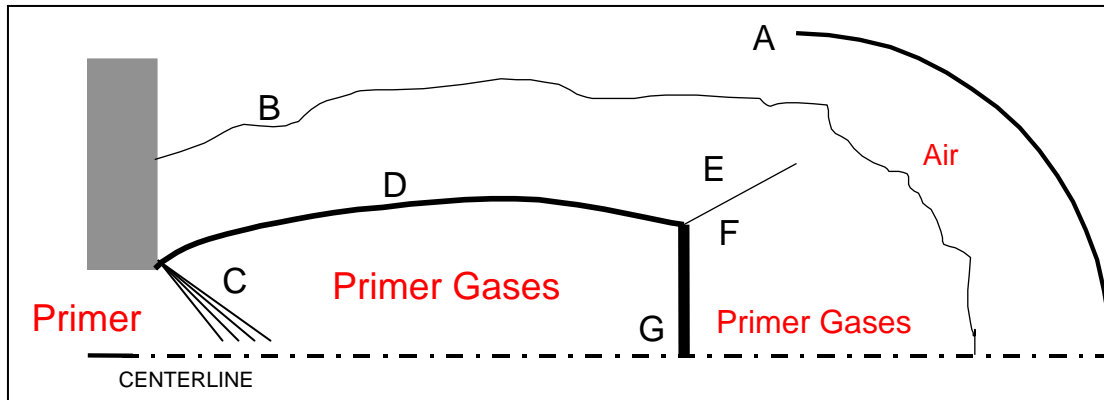
Figure 9. Schematic of gas dynamic features in a highly underexpanded jet.

Figures 10–13 show the time history of the primer efflux jet from shortly after entrance into the chamber (0.008 ms) to sometime after impact upon the opposite chamber wall and reflection back to the primer (0.144 ms). Note that the frames in figures 10–13 are not plotted to scale. Pressure contours are displayed in color-scale from 0 (blue) to 0.35 or 0.50 and above (red). Velocity vectors (not all vectors are displayed for clarity) are superimposed in order to indicate the magnitude (length of the vector) and direction of the local gas velocity. Mach number (local velocity normalized by the local sound velocity) contours (figure 8) are displayed in color-scale from 0 (blue) to 2.2 and above (red) with grey contour lines superimposed for emphasis.

As shown in figures 10 and 11, the high density and high pressure primer efflux enters the chamber as a highly underexpanded jet. Although not immediately evident in this scale, an expansion wave forms at the primer exit. A precursor shock is also formed from a mixture of air and primer gases (local molecular weight of about 30 g/mole) as the jet is moving at about 550 m/s at this time, about Mach 1.12 based on the local sound speed in the mixture. The primer gas from the orifice is of very high molecular weight, about 44 g/mole. The precursor shock is initially curved and shock reflections form on the chamber wall. By 0.022ms the leading edge of the precursor shock is nearly flat and the predominant gas dynamic features of the underexpanded jet have been established as seen more clearly when plotted at Mach number contours in figure 11. Curved barrel shocks emanate from the primer orifice terminating in a small Mach disk (at about 0.007 m in figure 11) and weak reflected shocks (the "X" patters near 0.007 m in figure 11). Supersonic flow resides within the barrel shocks and Mach disk (red color in figure 11). Due to the variable viscosity in the flowfield, the precursor shock is more diffuse than the normal shock of the Mack disk or the oblique barrel shock. Note the near sonic (i.e., Mach numbers subsonic to slightly supersonic) flow region between the normal shock and the precursor shock (green color); within this region resides the contact surface. Note that all of these features can be made more evident with a more highly refined computational mesh. The precursor shock impinges onto the projectile afterbody at about 0.037ms (figure 12) and reaches the end of the chamber before 0.072ms. In each case, a reflected shock is generated that

11

coalesces and moves back toward the primer, leaving behind near flow stagnation (note the absence of velocity vectors in the high pressure region shown in figure 12 for 0.072ms). A new high pressure flow region is formed on the chamber centerline at about midsection (see figure 12 for 0.072 ms) that results from the interaction of the Mach disk generated by the primer efflux and the receding reflected shock. Figure 13 shows the ultimate interaction of the reflected shock with the primer efflux jet near the jet orifice; the underexpanded jet is disturbed and then nearly reestablished by 0.144 ms. Note the formation of reverse flow along the chamber walls, forward flow along the chamber centerline and recirculation regions near the primer orifice at 0.101ms in figure 13. The primer jet is terminated at about 0.15 ms and subsequent gas dynamics in the chamber take the form of reflected waves and a steady buildup of pressure within the vessel. Eventually, the chamber flow is nearly uniform at a high level of pressure (not shown in these figures).
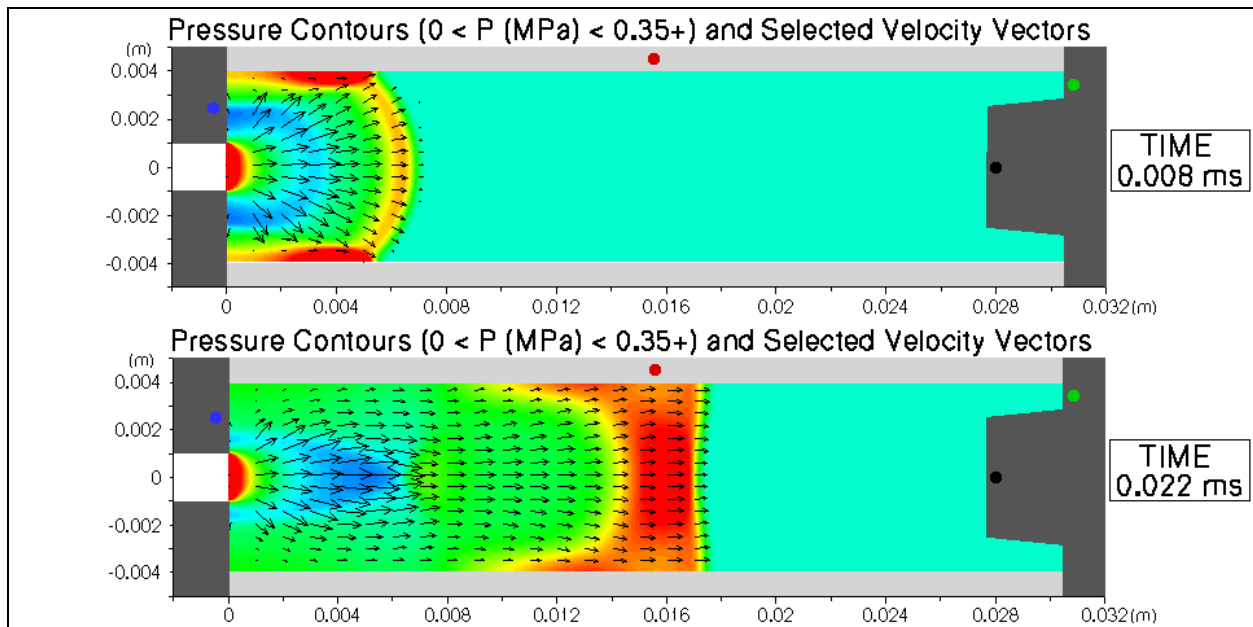
Figure 10. Computed color pressure contours and selected velocity vectors for 0.008 and 0.022 ms from initiation of the primer efflux.
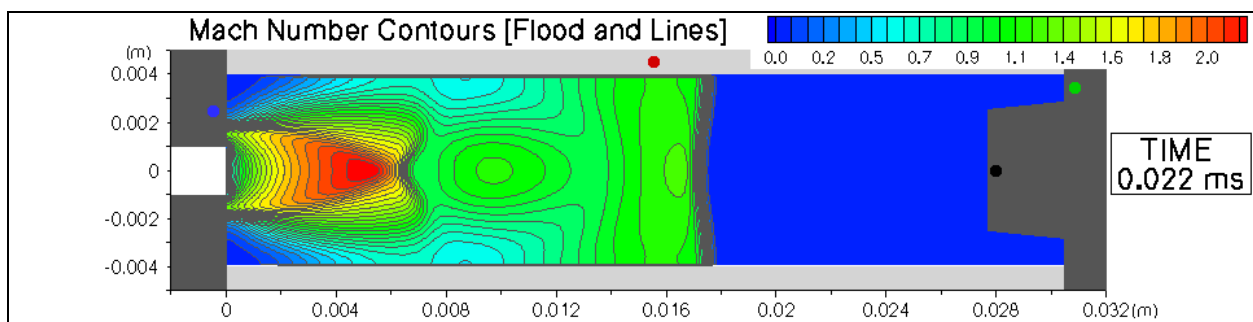
Figure 11. Computed color Mach number contours (with contour lines added) for 0.022 ms from initiation of the primer efflux.
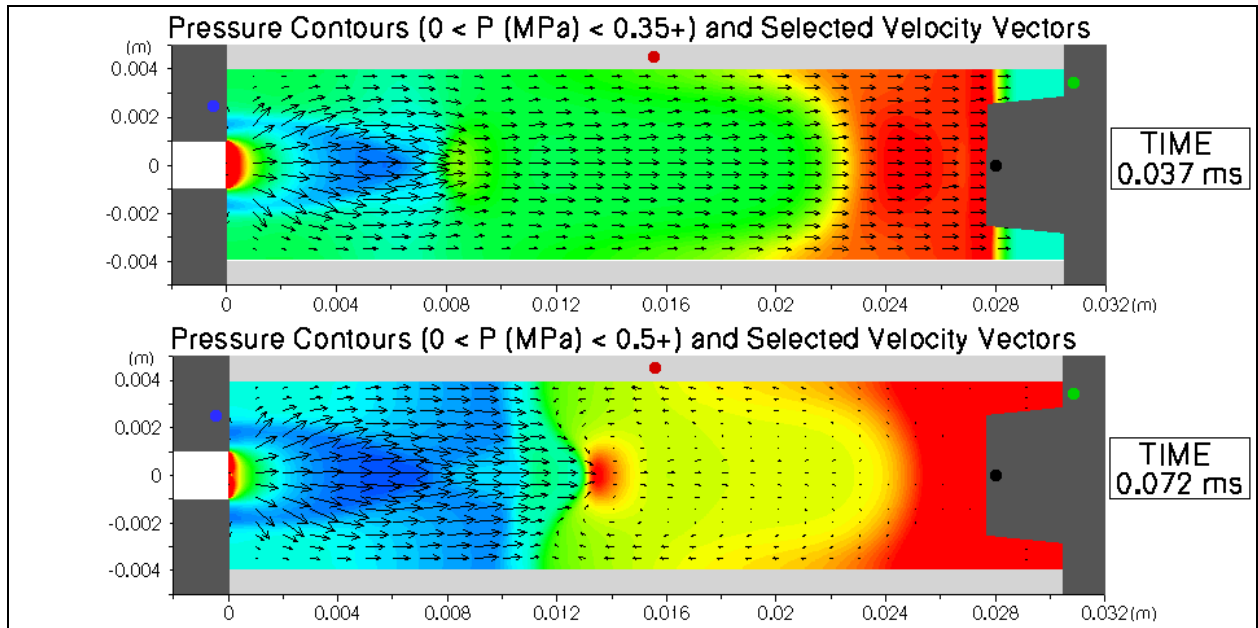
Figure 12. Computed color pressure contours and selected velocity vectors for 0.037 and 0.072 ms from initiation of the primer efflux.
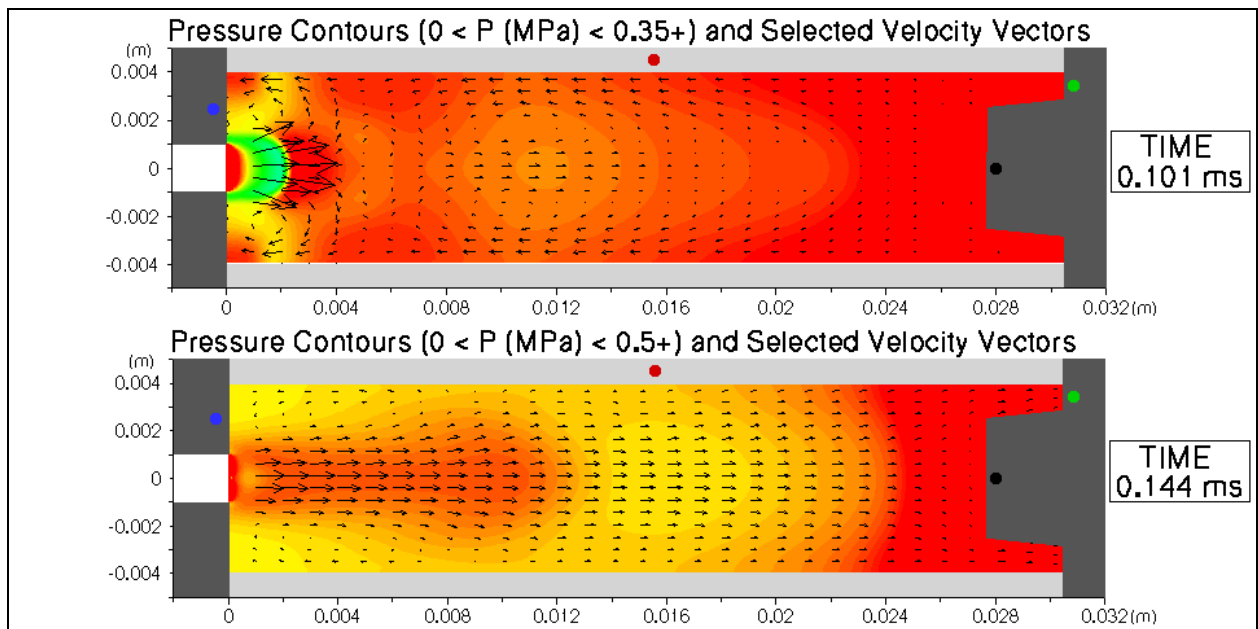
Figure 13. Computed color pressure contours and selected velocity vectors for 0.101 and 0.144 ms from initiation of the primer efflux.

Figure 14 shows the computed pressure-time histories as recorded at four wall-mounted pressure "taps" in the computational domain. Note the four colored "dots" in each of figures 10 through 13. At these locations, pressure was recorded while the simulation was executing; the line color

13

of figure 14 corresponds to these color dots. The pressure tap location, represented by the "black" dot, corresponds to the actual location of an experimental pressure tap with the data displayed in figure 4 and discussed in section 3. The arrival of the precursor shock onto the pressure tap mounted on the projectile afterbody (black curve in figure 14) is about 0.04 ms at a pressure level of about 2.6 MPa. Comparing these results to those displayed in figure 4, it can be said that the timing is similar and the computed pressure is about 13% low (measured value has an average value of 3 MPa). This indicated that perhaps the density of the primer efflux, used in the simulation, is too low. The other curves displayed in figure 14 provide an indication of the unsteady gas dynamics within the chamber as shock waves are generated and reflect from both radial and axial surfaces. Subsequent shock wave arrival and reflection from the pressure tap mounted on the projectile afterbody are evident in both the measured (figure 4) and computed (figure 14) results; however the computed results show a continual increase in pressure to a steady value of about 3.4 MPa at 4 ms, while the measured results show a steady or mean pressure level of about 1.5 MPa. It is postulated that some of this discrepancy is owed to heat losses to the walls and leaks or venting in the chamber during the experiment. These investigations will be the subject of future reports. Williams et al. (*15*) recorded optical images of the empty ballistic simulator which are consistent with the shock wave and its reflections as shown in the ARL-NSRG simulation figures 10–14.
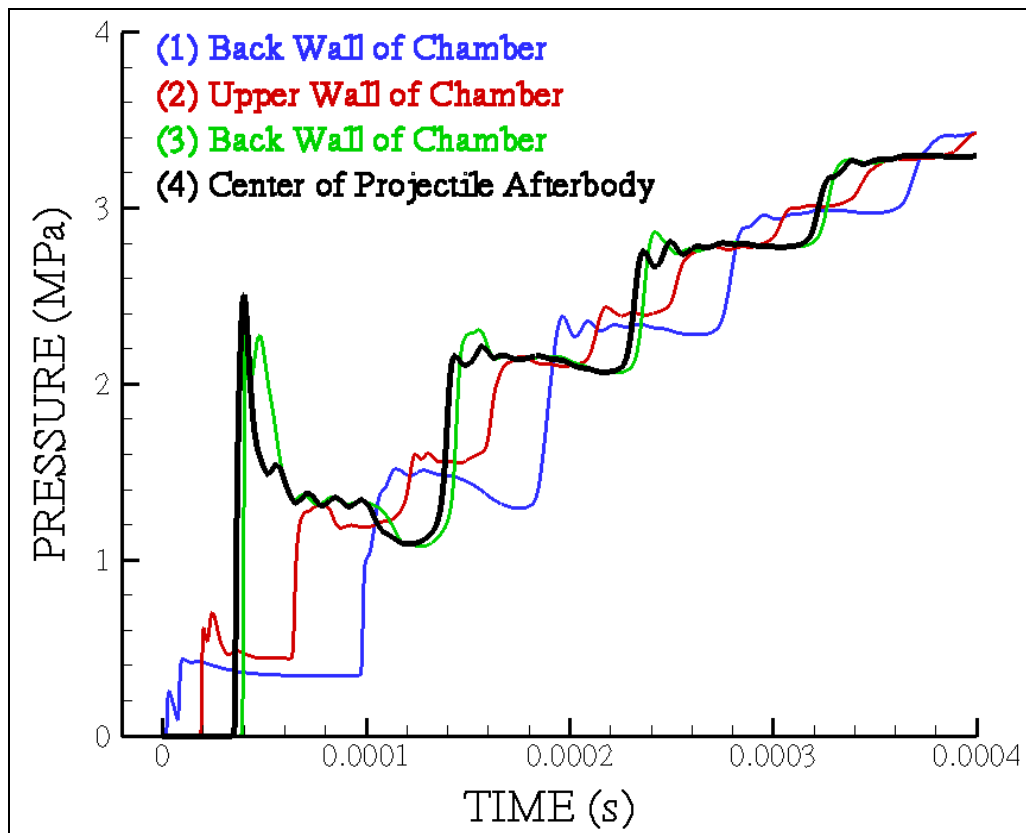
Figure 14. Computed pressure histories at four wall locations in the chamber, with color-coded lines that correspond to the locations noted in figures 10–13.

In order to gain an understanding of the dynamics of the 95 micron solid particles generated by the primer, computed results for the solid phase of the simulations are displayed in figures 15–17. These results are designed to be compared to the photographic evidence of the particles as given in figure 2. Since the model presently is not equipped with a way to graphically display the individual particles, a value of porosity is computed and graphed. In forming the porosity map for each point in time, each computational cell is interrogated for the presence of particles and since the diameter of these particles is known and is unchanging (in the current simulation the model's subroutines governing particle combustion are deactivated) the porosity is the ratio of cell volume occupied by the particles to the empty cell volume and then subtracted from unity. As a result, the red color (values approaching zero) of figures 15–17 indicates a high density of particles while the blue color (value of unity) of figures 15–17 indicates the absence of particles. Examining the time progression of figures 15 and 16 one observed a high density of particles that is quickly dispersed in a "fan"-like structure following the gas dynamic expansion and then is turned from the chamber wall as the flow features of the underexpanded jet are formed (discussed previously). Analysis of figure 15 time 0.006 ms shows a spreading angle of 72°. This is in good agreement with the measured spreading angle (yellow lines) of 70° shown in figure 2. Since the spreading angle is compared to an open air firing it was important to take measurements before the wall effects could influence the particle spreading angle. Figures 16 and 17 show that a small number of particles reach the chamber wall (and become trapped in the low velocity of the wall boundary layer) but most of the particles flow along with but lag the precursor shock. It should be noted that the individual "streamers" or "fingers" of particle are expected to coalescence in reality, but the fact that they do not is partially an artifact of the computational mesh used and mostly the fact that the particles are all given the identical initial conditions, with a zero velocity. The desire of the authors was to capture bulk flow properties of the particles in this simulation. Further simulations using particles and fluid with transient initial conditions are planned in the future. The expectation is that the finger structure, which is so evident in figures 15–17, will merge into a continuous distribution with turbulent initial conditions.
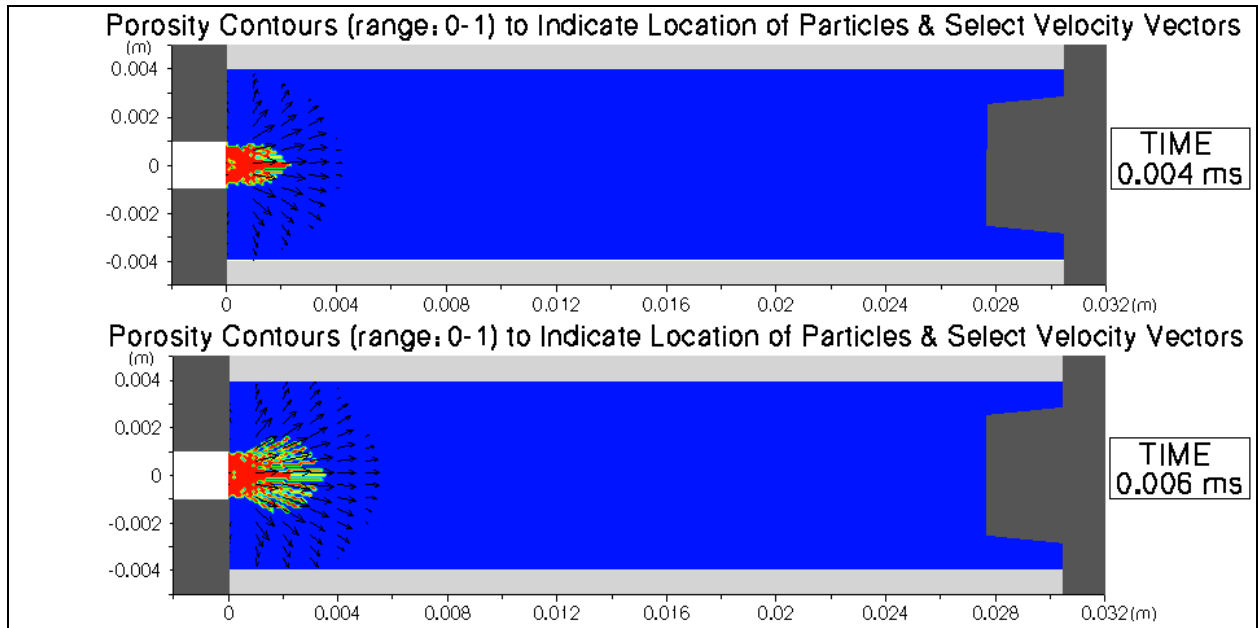
Figure 15. Computed color porosity contours (indicating location and density of solid particles) and selected velocity vectors for 0.004 and 0.006 ms from initiation of the primer efflux.
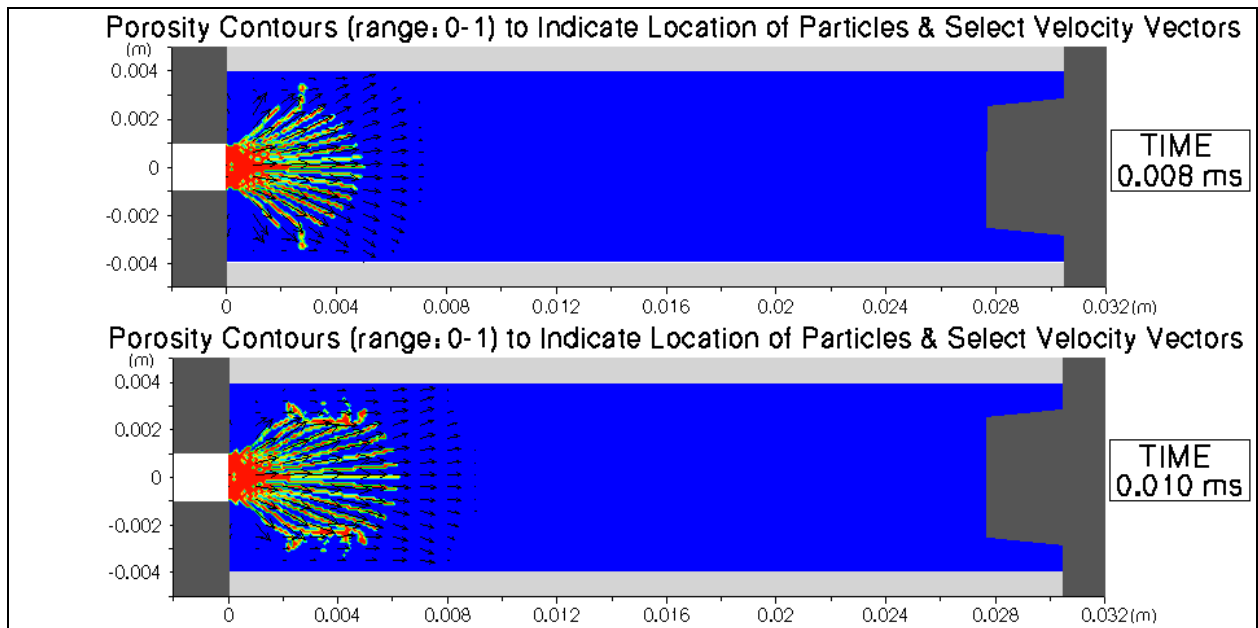
Figure 16. Computed color porosity contours (indicating location and density of solid particles) and selected velocity vectors for 0.008 and 0.010 ms from initiation of the primer efflux.

16
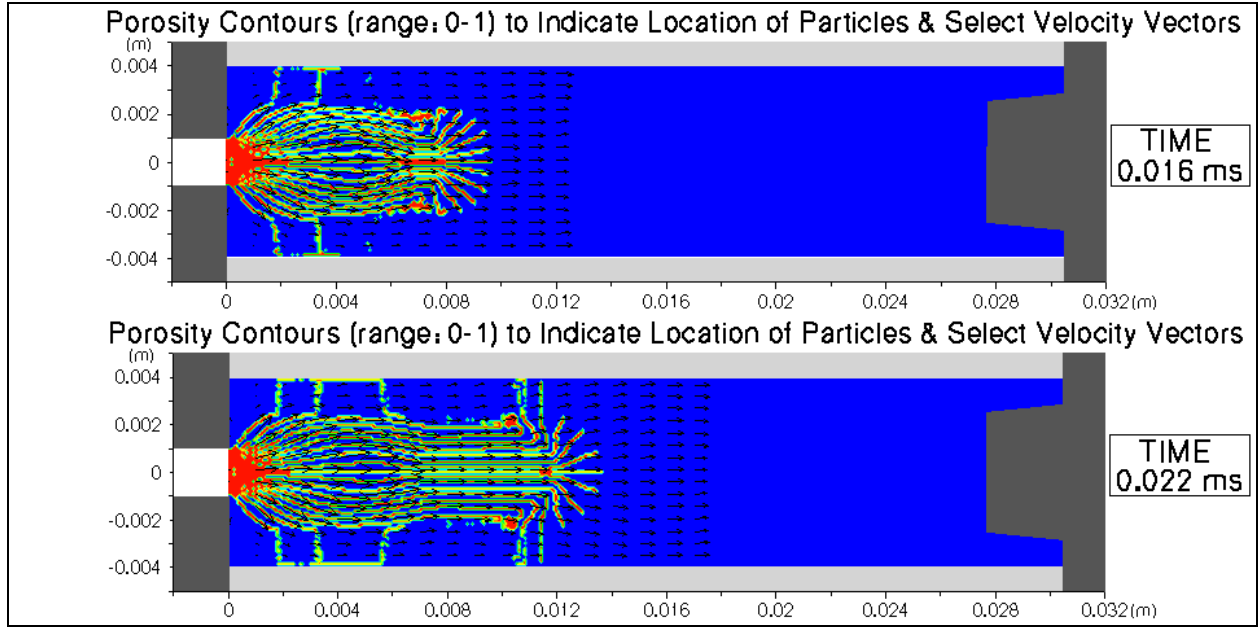
Figure 17. Computed color porosity contours (indicating location and density of solid particles) and selected velocity vectors for 0.016 and 0.022 ms from initiation of the primer efflux.

It is believed that the particle dynamics displayed in the modeling results are quite similar to those photographed (figure 2). However, additional quantitative work will be the subject of future reports, including a comparison of the computed and measured accumulation of particles deposited onto the projectile afterbody and the far axial wall of the chamber.

7. Conclusions

Analysis yielded a log-mean diameter of 95 microns for both the antimony sulfide and the barium nitrate. The primer tube was modeled at a steady-state turbulent channel flow with a $Re\tau = 356$. An analysis of particle behavior across the channel was consistent with trends shown in the literature; the higher the Stokes number the less sensitive the particles are to wall effects. Particle simulations were performed and converted to $R - \theta$ coordinates suitable for the ARL-NSRG code.

Coupling of the ARL-NSRG code with the statistically steady-state fluid phase velocity profile across the channel yielded characteristics of a classical under-expended jet. Simulated pressure taps showed properties that are consistent with measurements. An average measured peak pressure of 3 MPa was recorded between 0.03 and 0.04 ms. This simulation showed a peak pressure of 2.6 MPa at 0.04 ms; this was considered acceptable agreement considering the assumptions made. The experimental data showed a rapid decay of pressure levels to a steady value that was notably lower than the computed value; the computed pressure shows a gradual rise to a steady pressure. The discrepancy between measured and computed results is mostly

17

attributed to the fact that the experiment had heat losses to the surroundings, but the simulation was adiabatic. Also, the fact that the experimental chamber reverted back to atmospheric pressure shortly after the firing event probably indicates that there were leaks in the experimental apparatus.

A steady stream of particles was fed into the ARL-NSRG simulation with identical zero initial conditions. The particles were evenly distributed across the opening. Analysis of the initial particle spreading angle yielded a close match to the measured spreading angle of an open air firing, 72° compared to 70°, respectively.

Finger-like structures were seen in the simulations indicating an ordering of the particles that is not considered realistic. The finger structure is attributed to (1) the mesh size and (2) the ordered initial conditions. The introduction of particles with transient initial conditions (via the ODT simulation) is expected to alleviate most of this artifact.

The optical images of the empty ballistic simulator obtained by Williams et al. (*15*) are consistent with the ARL-NSRG simulations.

References

1. Anderson, R.; Fickie, K. *IBHGV2 – A User's Guide*; BRL-TR-2829; U.S. Army Ballistic Research Laboratory: Aberdeen Proving Ground, MD, July 1987.

2. Gough, P. S. *Interior Ballistics Modeling: Extensions to the XKTC Code and Analytical Studies of Pressure Gradient for Lumped Parameter Codes*; ARL-CR-460; U.S. Army Research Laboratory: Aberdeen Proving Ground, MD, February 2001.

3. Minor, T. C.; Horst, A. W. *Theoretical and Experimental Investigation of Flamespreading Processes in Combustible-Cased Stick Propelling Charges*; BRL-TR-2710; U.S. Army Ballistic Research Laboratory: Aberdeen Proving Ground, MD, February 1986.

4. Gough, P. S. Modeling Arbitrarily Packaged Multi-Increment Solid Propellant Charges of Various Propellant Configurations. *Proceedings of the 33rd JANNAF Combustion Meeting*, CPIA Pub. 653, Vol. 1, pp 421-435, November 1996 (see also Gough, P.S. *Formulation of a Next-Generation Interior Ballistic Code*; ARL-CR-68; U.S. Army Research Laboratory, September 1993).

5. Nusca, M. J.; Gough, P. S. *Numerical Model of Multiphase Flows Applied to Solid Propellant Combustion in Gun Systems*, AIAA Paper No. 98-3695, July 1998.

6. Nusca, M. J. *High-Performance Computing and Simulation for Advanced Armament Propulsion*; ARL-TR-3215; U.S. Army Research Laboratory: Aberdeen Proving Ground, MD, June 2004.

7. Horst, A. W.; Nusca, M. J. *The Charge Designer's Workbench: A Range of Interior Ballistic Modeling Tools*; ARL-TR-3796; U.S. Army Research Laboratory: Aberdeen Proving Ground, MD, May 2006.

8. Gough, P. S. Modeling Chemical Interactions in Ignition of Gun Propellants. *Proceedings of the 22nd JANNAF Combustion Meeting*, Pasadena, CA, CPIA Publication No. 432, Vol. 1, October 1983.

9. Keller, G. E.; Horst, A. W. *The Two Phase Flow Simulation of LOVA Propellant Interior Ballistic Behavior Using the XNOVAK Code*; BRL-TR-2796; U.S. Army Ballistic Research Laboratory: Aberdeen Proving Ground, MD, April 1987.

10. Davis, Tenney L. *The Chemistry of Powder and Explosives*, John Wiley & Sons, Inc.: New York, 1943.

11. Ekstedt, E. E.; Vest, D. C.; Emerson, V. C.; Dean, L. W. *Pressure Studies of Artillery Primers Fired Statically*; BRL Report No. 938; U.S. Army Ballistic Research Laboratory: Aberdeen Proving Ground, MD, June 1955, p 9.

12. Chang, L.-M.; Rocchio, J. J. *Simulator Diagnostics of the Early Phase Ignition Phenomena in a 105-mm Tank Gun Chamber*; BRL-TR-2890; U.S. Army Ballistic Research Laboratory: Aberdeen Proving Ground, MD, March 1988.

13. Schmidt, J. R.; Nusca M. J. Progress in the Development of a Multiphase Turbulent Model of the Gas/Particle Flow in the Primer Tube for Small Caliber Ammunition. *Proceeding of the 53rd JANNAF Propulsion Meeting*, CPIAC JPMCD05, Monterey, CA, December 2005.

14. Schmidt, J. R.; Nusca M. J. *Progress in the Development of a Multiphase Turbulent Model of the Gas/Particle Flow in a Small Caliber Ammunition Primer*; ARL-TR-3860; U.S. Army Research Laboratory: Aberdeen Proving Ground, MD, August 2006.

15. Williams, A. W.; Brant, A. L.; Kaste, P. J.; Colburn, J. W. Experimental Studies of Primer Ignition in 5.56-mm Ammunition. *Proceeding of the 53rd JANNAF Propulsion Meeting*, CPIAC JPMCD05, Monterey, CA, December 2005.

16. Williams, A. W.; Brant, A. L.; Kaste, P. J.; Colburn, J. W. *Experimental Studies of the No. 41 Primer and Ignition of 5.56-mm Ammunition*; ARL-TR-3922; U.S. Army Research Laboratory: Aberdeen Proving Ground, MD, August 2006.

17. Nusca, M. J. Numerical Simulation of Electromagnetic Wave Attenuation in Nonequilibrium Chemically Reacting Flows. *Computers and Fluids* **1998**, *27* (2), 217–238.

18. Nusca, M. J. Numerical Simulation of the Ram Accelerator Using a New Chemical Kinetics Mechanism. *J. of Propulsion and Power* **January-February 2002**, *18* (1), 44–52.

19. Nusca, M. J.; McQuaid, M. J.; Anderson, W. R. Numerical Model of the Plasma Jet Generated by an Electrothermal-Chemical Igniter. *J. of Thermophysics and Heat Transfer*, **January-March 2002**, *16* (1), 44–52.

20. Nusca, M. J.; Anderson, W. R.; McQuaid, M. J. *Multispecies Reacting Flow Model for the Plasma Efflux of an ETC Igniter – Application to an Open-Air Plasma Jet Impinging on an Instrumented Probe*; ARL-TR-3227; U.S. Army Research Laboratory: Aberdeen Proving Ground, MD, July 2004.

21. Nusca, M.J.; Anderson, W.R.; McQuaid, M.J. *Multispecies Reacting Flow Model for the Plasma Efflux of an ETC Igniter – Application to an Open-Air Plasma Jet Impinging on an Instrumented Plate*; ARL-TR-3275; U.S. Army Research Laboratory: Aberdeen Proving Ground, MD, August 2004.

22. Nusca, M. J.; Mathis, N. P.; Michaels, R. S. *Modeling Hypergolic Ignition in the Army's Impinging Stream Vortex Engine Including Injection Throttling*, 43rd AIAA/ASME/SAE/ASEE Joint Propulsion Conference & Exhibit, Cincinnati, OH, July 2007.

23. Nusca, M. J. *Utility of Computational Modeling for the Study of Combustion Instability in Small MMH-NTO Liquid Rocket Engines*, 43rd AIAA/ASME/SAE/ASEE Joint Propulsion Conference & Exhibit, Cincinnati, OH, July 2007.

24. Shaw, R. W.; Mann, D. M.; Anderson, W. R.; White, K. J.; Nusca, M. J.; Powell, J. *Army Plasma/Propellant Interaction Workshop – U.S. Army Research Office, 17-18 November 1998*; ARL-SR-83; U.S. Army Research Laboratory: Aberdeen Proving Ground, MD, November 1999.

25. Schmidt, J. R. Stochastic Models for the Prediction of Individual Particle Trajectories in One Dimensional Turbulence Flows, PhD Dissertation The University of Arizona, Tucson, Arizona 2004.

Acronyms

ARL   U.S. Army Research Laboratory

BRL   Ballistics Research Laboratory

CFD   computational fluid dynamics

D   dimensional

EDAX   Energy-Dispersive X-ray spectroscopy

FTIR   Fourier Transform Infrared spectroscopy

IB   interior ballistics

JWL   Jones-Wilkins-Lee equation of state

MAS   Maneuver Ammunition Systems

Mil   Military

NASA   National Aeronautics and Space Administration

NSRG   Navier-Stokes Real Gas

ODT   One Dimensional Turbulence

PETN   pentaerythritoltetranitrate

PM   Program Manager

Re   Reynolds number

SEM   Scanning Electron Microscope

1 (PDF) ADMNSTR
only) DEFNS TECHL INFO CTR
DTIC OCP (ELECTRONIC COPY)
8725 JOHN J KINGMAN RD STE 0944
FT BELVOIR VA 22060-6218

1 US MILITARY ACADEMY
MATH SCI CTR EXCELLENCE
ATTN   MADN MATH
        MAJ HUBER
THAYER HALL
WEST POINT NY 10996-1786

3 DIRECTOR
US ARMY RESEARCH LAB
IMNE ALC IMS MAIL&RECORDS MGMT
AMSRD ARL CI OK TL TECHL LIB
AMSRD ARL CI OK T TECHL PUB
2800 POWDER MILL RD
ADELPHI MD 20783-1197

1 DIRECTOR
US ARMY RESEARCH LAB
ATTN AMSRD ARL CI AI R
2800 POWDER MILL RD
ADELPHI MD 20783-1197

3 DIRECTOR
US ARMY RESEARCH LAB
ATTN AMSRD ARL CI LL
2800 POWDER MILL RD
ADELPHI MD 20783-1197

3 DIRECTOR
US ARMY RESEARCH LAB
ATTN   AMSRD ARL RO P
        D MANN
        R SHAW
        TECH LIB
PO BOX 12211
RSRCH TRIANGLE PARK NC 27709-2211

3 US ARMY AVIATN & MSLE CMD
ATTN   AMSRD AMR PS PT
        W CHEW
        C DOLBEER
        J S LILLY
        M LYON
        J M FISHER
        B P MARSH
        R S MICHAELS
        D THOMPSON
REDSTONE ARSENAL AL 35898-5249

2 PM MAS
ATTN   SFAE AMO MAS
        LTC M BUTLER
PICATINNY ARSENAL NJ 07806-5000

2 PM CAS
ATTN   SFAE AMO CAS
PICATINNY ARSEBAL NJ 07806-5000

16 CDR US ARMY ARDEC
ATTN   C ADAM
        D CARLUCCI
        R CARR
        R CIRINCIONE
        S EINSTEIN
        T GORA
        P HUI
        J LANNON
        E LOGSDEN
        P LU
        B MACHAK
        S NICHOLICH
        P O'REILLY
        J O'REILLY
        J RUTKOWSKI
        A SABASTO
        J SHIN
        R SURAPANENI
PICATINNY ARSENAL NJ 07806-5000

8	DIR BENET WEAPONS LAB
	ATTN M AUDINO
	        R DILLON
	        R FISCELLA
	        R HASENBEIN
	        E KATHE
	        K MINER
	        S SOPOK
	        J MCNEIL
	WATERVLIET NY 12189-4000

1   COMMANDER
RADFORD ARMY AMMO PLANT
ATTN SMCAR QA HI LIB
RADFORD VA 24141-0298

1   COMMANDANT
USAFC&S
ATTN ATSF CN P GROSS
FT SILL OK 73503-5600

2   CDR NAVAL RSRCH LAB
ATTN   TECH LIBRARY
          J BORIS
WASHINGTON DC 20375-5000

1   OFFICE OF NAVAL RSRCH
ATTN J GOLDWASSER
875 N RANDOLPH ST RM 653
ARLINGTON VA 22203-1927

6   CDR
NAVAL SURFACE WARFARE CENTER
ATTN   R2A   R DOHERTY
          TM3   C GOTZMER
          R22   C MICHIENZI
          OPA   S MITCHELL
          R3A   S C SMITH
          TECHLIB
INDIAN HEAD MD 20640-5000

5   CDR
NAVAL SURFACE WARFARE CTR
ATTN   J FRAYSEE
          R FRANCIS
          T C SMITH
          T TSCHIRN
          TECHLIB
DAHLGREN VA 22448-5000

3   CDR
NAVAL AIR WARFARE CTR
ATTN   A ATWOOD
          S BLASHILL
          T PARR
CH1NA LAKE CA 93555-6001

1   AIR FORCE RESH LAB
ATTN   MNME EN MAT BR
          B WILSON
2306 PERIMETER RD
EGLIN AFB FL 32542-5910

1   AIR FORCE OFC OF SCI RSRCH
ATTN M BERMAN
875 N RANDOLPH ST
SUITE 235 RM 3112
ARLINGTON VA 22203-1768

1   NASA LANGLEY RSRCH CENTER
ATTN D BUSHNELL
MAIL STOP 110
HAMPTON VA 23681-2199

1   DIR SANDIA NATL LABS
ATTN M BAER DEPT 1512
PO BOX 5800
ALBUQUERQUE NM 87185

2   DIR LAWRENCE LIVERMORE NL
ATTN   L FRIED
          M MURPHY
PO BOX 808
LIVERMORE CA 94550-0622

1   CENTRAL INTELLIGENCE AGNCY
ATTN J BACKOFEN
RM 4PO7 NHB
WASHINGTON DC 20505

1   BATTELLE EAST SCI & TECH
ATTN A ELLIS
1204 TECHNOLOGY DRIVE
ABERDEEN MD 21001-1228

2   JHU CHEM PROP INFO AGNCY
ATTN   W HUFFERD
          R FRY
10630 LITTLE PATUXENT PKWY
STE 202
COLUMBIA MD 21044-3200

1	OUSD (AT&L)/STRAT & TACT SYS MUNITIONS ATTN T MELITA 3090 DEFENSE PENTAGON RM 3B1060 WASHINGTON DC 20301-3090
1	BRIGHAM YOUNG UNIV ATTN M BECKSTEAD DEPT OF CHEMICAL ENGRG PROVO UT 84601
1	CALIF INSTITUTE OF TECHLGY ATTN F E C CULICK 204 KARMAN LAB MAIL STOP 301 46 1201 E CALIFORNIA ST PASADENA CA 91109
2	UNIV OF ILLINOIS DEPT OF MECH INDUSTRY ENGINEERING ATTN H KRIER R BEDDINI 144 MEB 1206 N GREEN ST URBANA IL 61801-2978
4	PENNSYLVANIA STATE UNIV DEPT OF MECHANICAL ENGRG ATTN K KUO T LITZINGER G SETTLES S THYNELL V YANG UNIVERSITY PARK PA 16802-7501
1	INST FOR ADVNCD TECHNLGY 3925 W BRAKER LN SUITE 400 AUSTIN TX 78759-5316
1	ARROW TECHLGY ASSOC INC 1233 SHELBURNE RD D 8 SOUTH BURUNGTON VT 05403
1	ALLEGHENY BALLISTICS LAB PO BOX 210 ROCKET CENTER WV 26726
1	ATK ORDNANCE 4700 NATHAN LANE PLYMOUTH MN 55442

3	ATK AMMO & ENERGETICS ATTN D A WORRELL W J WORRELL S RITCHIE RADFORD ARMY AMMO PLANT ROUTE 114 PO BOX 1 RADFORD VA 24141-0299
4	ATK THIOKOL ATTN P BRAITHWAITE T B FARABAUGH W B WALKUP R WARDLE PO BOX 707 BRIGHAM CITY UT 84302-0707
1	ATK ELKTON ATTN J HARTWELL PO BOX 241 ELKTON MD 21921-0241
1	BAE ARMAMENT SYS DIV ATTN JAHN DYVIK 4800 EAST RIVER RD MINNEAPOLIS MN 55421-1498
2	GEN DYNAMICS ORD/TACT SYS ATTN N HYLTON J BUZZETT 10101 DR M L KING ST N ST PETERSBURG FL 33716
3	GENERAL DYNAMICS ST MARKS ATTN J DRUMMOND H RAINES D W WORTHINGTON PO BOX 222 SAINT MARKS FL 32355-0222
1	GENERAL DYNAMICS ARM SYS ATTN J TALLEY 128 LAKESIDE AVE BURLINGTON VT 05401
1	HICKS AND ASSOCIATES SAIC ATTN I MAY 7990 SCIENCE APPLIC CT VIENNA VA 22182
1	PAUL GOUGH ASSOC INC P S GOUGH 1048 SOUTH ST PORTSMOUTH NH 03801-5423

3   VERITAY TECHGY INC
               R SALIZONI
               J BARNES
               E FISHER
        4845 MILLERSPORT HWY
        EAST AMHERST NY 14501-0305

1   SRI INTERNATIONAL
        PROPULSION SCIENCES DIV
        ATTN TECH LIB
        333 RAVENWOOD AVE
        MENLO PARK CA 94025-3493

1   SAIC
        ATTN M PALMER
        1410 SPRING HILL RD
        SUITE 400
        MCLEAN VA 22102

1   NETWORK COMPUTING SERVICES
        ATTN S RAY
        1200 WASHINGTON AVE S
        MINNEAPOLIS MN 55415

1   CDR USA ATC
        STECS LI R HENDRICKSEN
        APG MD 21005

1   SANDIA NATIONAL LABS
        ATTN A KERSTEIN
        PO BOX 969 MS 9051
        LIVERMORE CA 94551-0969

ABERDEEN PROVING GROUND

68   DIR USARL
    AMSRD CI OK TP
      TECHL LIB
    AMSRD ARL WM
      T ROSENBERGER
    AMSRD ARL WM M
      S MCKNIGHT
    AMSRD ARL WM T
      B BURNS
    AMSRD ARL WM TB
      P BAKER
    AMSRD ARL WM BD
      R D ANDERSON
      W R ANDERSON
      R A BEYER
      A L BRANT
      G BROWN
      M BUNDY
      S W BUNTE
      C CANDLAND
      W CIEPIELA
      G COOPER
      L M CHANG
      T P COFFEE
      J COLBURN
      P J CONROY
      B DAVIS
      J DESPIRITO
      N ELDREDGE
      B E FORCH
      J GARNER
      D HEPNER
      B E HOMAN

      AW HORST
      S L HOWARD
      P J KASTE
      G KATULKA
      T KOGLER
      A J KOTLAR
      C LEVERITT
      R LIEB
      D LYON
      K L MCNESBY
      M MCQUAID
      M S MILLER
      A W MIZIOLEK
      J B MORRIS
      J A NEWBERRY
      J NEWILL
      M J NUSCA (6 copies)
      W OBERLE
      R A PESCE-RODRIGUEZ
      P PLOSTINS
      S PIRIANO
      G P REEVES
      B M RICE
      J SAHU
      R C SAUSA
      S SILTON
      E SCHMIDT
      J SCHMIDT (6 copies)
      P WEINACHT
      D WILKERSON
      A W WILLIAMS
      M ZOLTOSKI

Total   (179 HCs, 1 PDF)

INTENTIONALLY LEFT BLANK.